Supplementary Materials and Methods

Gene-expression analyses. Population-level and single-cell RNA-seq and microarray analyses were performed using published datasets (1-5). Population-level RNA-seq analyses were performed in edgeR (v3.34.0) using the quasi-likelihood F-test ('glmQLFTest') for differential expression (6). scRNA-seq analysis was performed in Seurat (v4.0.2) using the function 'FindMarkers' for differential expression, with the following parameters: 'only.pos=F, logfc.threshold=0.0, min.pct=0, test.use=DESeq2' (7). For comparison of *Ctla4*$^{+}$ vs *Ctla4*$^{-}$ mTECs, pooled *Ctla4*$^{+}$ mTECs from *Aire*$^{+/+}$ and *Aire*$^{-/-}$ mice were used for maximal statistical power. Microarray analysis was performed in R (v4.1.0). p-values were adjusted for multiple comparisons by the Benjamini-Hochberg method where indicated. Gene ontology analysis was performed using the online tool g:Profiler (www.biit.cs.ut.ee/gprofiler).

Mice. All mouse work was performed according to the Harvard Animal Care and Use Committee guidelines under protocol #IS00001257. We used the following strains: C57BL/6J (JAX #000664), B6.*Aire*$^{-/-}$ (our colony), B6.*Foxn1-cre* (JAX #018448), B6.*Ctla4-flox* (gift from Dr. Arlene Sharpe) and B6.*Rag1*$^{-/-}$ (JAX #002216). Littermates were used for comparisons of WT and KO mice. Mice were examined at 4-6 weeks of age unless otherwise specified. Both male and female mice were used for most experiments after confirming that there was no evident difference in phenotype between the sexes. For autoantibody and histologic analyses, male mice were used to control for sex-specific autoimmune effects. Mice were housed under specific-pathogen-free conditions.

Immunofluorescence microscopy. Thymi were dissected and fixed for 1 hour in 4% paraformaldehyde, then flash frozen in OCT and sectioned at 8μm onto slides. Sections were permeabilized in phosphate buffered saline (PBS) plus 0.05% Tween-20 (PBS-T), blocked for 1 hour at room temperature (RT) with rat serum in PBS-T, incubated with conjugated primary antibodies against CTLA-4 and EpCAM (both Biolegend) for 1 hour at RT, washed in PBS-T, counterstained with Hoescht 33242 (Sigma) and mounted for imaging. Images were acquired by spinning disk confocal microscopy using a Nikon Ti inverted microscope, W1 Yokogawa spinning disk with 50mm pinholes and Plan Apo 20X air and 60X oil objectives.

Autoimmune monitoring, serum autoantibodies and histology. *Ctla4*$^{\Delta TEC}$ mice were observed at least once per week from weaning through the duration of the monitoring period. At sacrifice, serum was collected and organs removed. Autoantibody analysis was performed as previously described (8). Briefly, serum was separated from blood cells, stored at -80°C, and used at a 1:500 dilution to stain Western blots of various organ lysates from *Rag1*$^{-/-}$ mice, followed by visualization using horseradish-peroxidase-conjugated donkey anti-mouse IgG (Jackson ImmunoResearch) and ECL Prime reagent (Amersham). Autoantibody signal was quantitated for each mouse in ImageJ (v1.52) by calculating the signal over background for each lane. For histologic analysis, organs were placed in 10% formalin, embedded, sectioned and stained by hematoxylin and eosin by the Harvard Medical School Rodent Histopathology Core. Slides were scored for immunocyte infiltration and tissue destruction on a scale from 0 (no infiltration or

destruction) to 4 (severe infiltration and destruction) by two independent, blinded evaluators. The pathologic score for each slide was calculated as the mean of the two scores. Histology images were acquired by brightfield microscopy using a Nikon Ti inverted microscope and a Plan Apo 10X air objective.

Supplementary Figure Legends

Figure S1: Additional characterization of CTLA-4 expression by mTECs

(A) Volcano plots of two independent datasets of bulk RNA-seq of mTEC^{hi} from *Aire*$^{+/+}$ vs *Aire*$^{-/-}$ mice. Each dot represents one gene, and differentially expressed genes (FDR<0.05) are highlighted in red and blue. Data were reanalyzed from (4) (top) and (2) (bottom).

(B) Boxplots showing expression of *Ctla4* in mTEC^{hi} from *Aire*$^{+/+}$ vs *Aire*$^{-/-}$ mice on the C57BL/6 (n=3 vs n=3, left) and BALB/c (n=3 vs n=4, right) genetic backgrounds, as assayed by microarray. Each dot represents one mouse, and boxplots show median and interquartile range (IQR) as boxes and minimum and maximum values (up to ±1.5*IQR) as whiskers. Data were reanalyzed from (1).

(C) Gating strategy for mTEC^{hi}. Representative isotype control and CTLA-4 staining in mTEC^{hi} from *Aire*$^{+/+}$ and *Aire*$^{-/-}$ mice are shown at the far right.

(D) Expression of *Ctla4* in pre-Aire mTEC^{lo} (n=3), Aire-stage mTEC^{hi} (n=3) or post-Aire mTEC^{lo} (n=3), as assayed by bulk RNA-seq. Each dot represents one mouse, and boxplots were generated as in (B). Data were reanalyzed from (5).

(E) Summarized flow cytometry data of CTLA-4 levels (gMFI) in mTEC^{hi} from *Aire*$^{+/+}$ (n=6) vs *Aire*$^{-/-}$ (n=4) mice. Each dot represents one mouse, data are representative of at least two independent experiments, p-value was calculated by two-sided, unpaired Student's t-test, and bars represent mean ± SEM.

Figure S2: Additional characterization of splenocytes, thymocytes and thymic APCs from *Ctla4$^{\Delta TEC}$ mice*

(A) Flow cytometry plots (left) and summarized data (right) of CTLA-4 expression on mTEC^{hi} from *Ctla4^{fl}* (n=5) and *Ctla4$^{\Delta TEC}$* (n=4) mice.

(B) Gating strategy for splenic T cell subsets.

(C, D) Numbers of (C) total splenocytes and (D) activated (CD44^{hi}CD62L^{lo}) Tregs in spleens from *Ctla4^{fl}* (n=5) and *Ctla4$^{\Delta TEC}$* (n=4) mice. Each dot represents one mouse, data are representative of at least two independent experiments, and bars represent mean ± SEM.

(E) Gating strategy for thymocyte subsets and Treg progenitors.

(F, G) Numbers of (F) total thymocytes and (G) CD25^{-}Foxp3^{+} Treg progenitors in thymi from *Ctla4^{fl}* (n=12) and *Ctla4$^{\Delta TEC}$* (n=12) mice. Each dot represents one mouse, data are pooled from two independent experiments, and bars represent mean ± SEM.

(H) Gating strategy for thymic cDCs, pDCs and B cells.

Figure S3: Immunoblots of autoantibodies from *Ctla4^{fl}* and *Ctla4$^{\Delta TEC}$* mice

Immunoblots of lysates from the indicated organs stained with sera from 1-year-old *Ctla4^{fl}* (n=4, left lanes) vs *Ctla4$^{\Delta TEC}$* (n=4, right lanes) mice. Each vertical lane represents one mouse.

Supplementary References

1. E. S. Venanzi, R. Melamed, D. Mathis, C. Benoist, The variable immunological self: genetic variation and nongenetic noise in Aire-regulated transcription. *Proc Natl Acad Sci U S A* **105,** 15860-15865 (2008).

2. S. N. Sansom, et al., Population and single-cell genomics reveal the Aire dependency, relief from Polycomb silencing, and distribution of self-antigen expression in thymic epithelia. *Genome Res.* **24,** 1918-1931 (2014).

3. M. Meredith, D. Zemmour, D. Mathis, C. Benoist, Aire controls gene expression in the thymic epithelium with ordered stochasticity. *Nat Immunol* **16,** 942-949 (2015).

4. K. Bansal, et al., Aire regulates chromatin looping by evicting CTCF from domain boundaries and favoring accumulation of cohesin on superenhancers. *Proc Natl Acad Sci U S A* **118,** e2110991118 (2021).

5. D. A. Michelson, et al., Thymic epithelial cells co-opt lineage-defining transcription factors to eliminate autoreactive T cells. *Cell* **185,** 2542-2558 (2022).

6. M. D. Robinson, D. J. McCarthy, G. K. Smyth, edgeR: a Bioconductor package for differential expression analysis of digital gene expression data. *Bioinformatics.* **26,** 139-140 (2010).

7. Y. Hao, et al., Integrated analysis of multimodal single-cell data. *Cell* **184,** 3573-3587 (2021).

8. M. S. Anderson, et al., Projection of an immunological self shadow within the thymus by the aire protein. *Science* **298,** 1395-1401 (2002).

Supplementary Fig 1

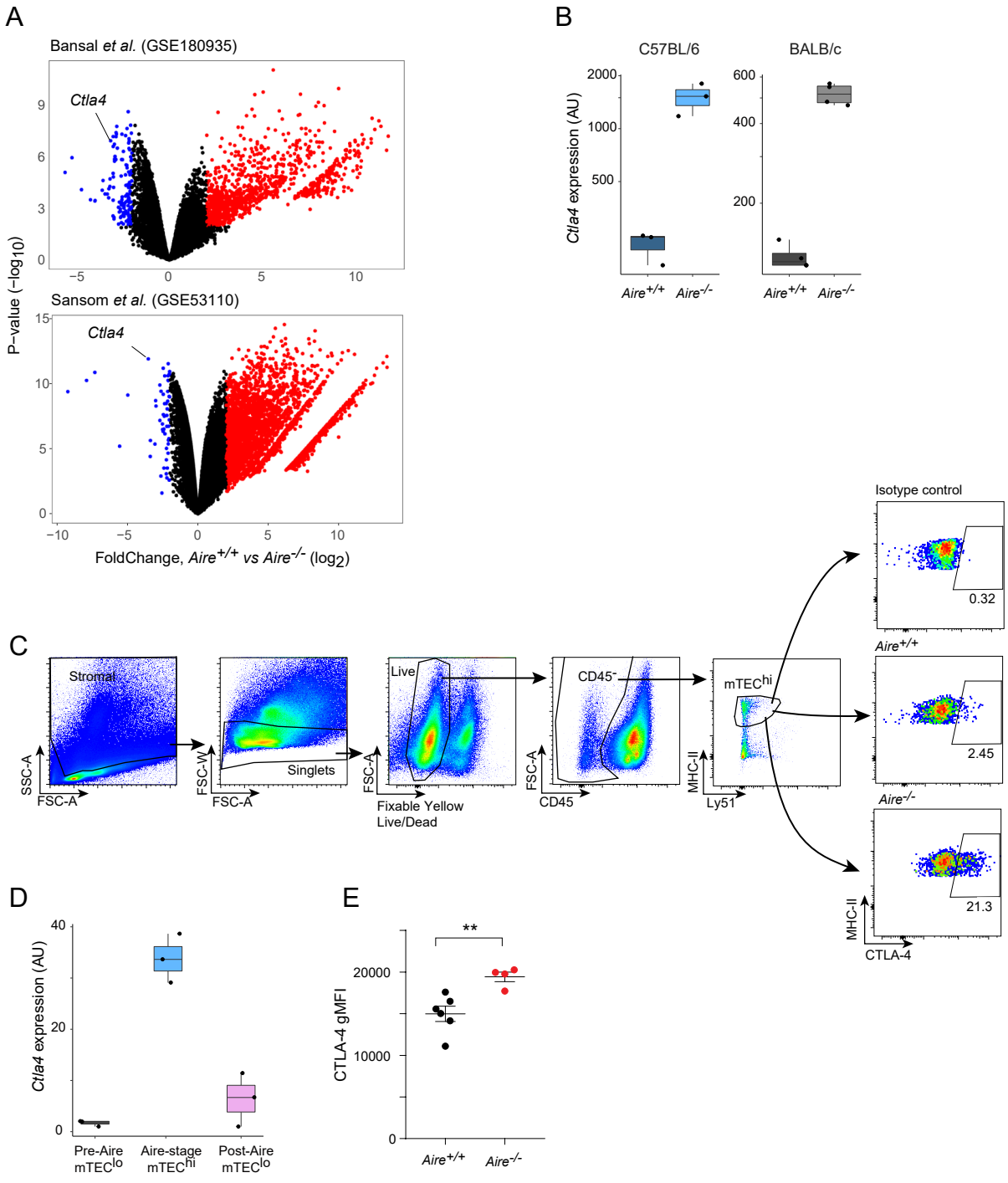

Supplementary Fig 2

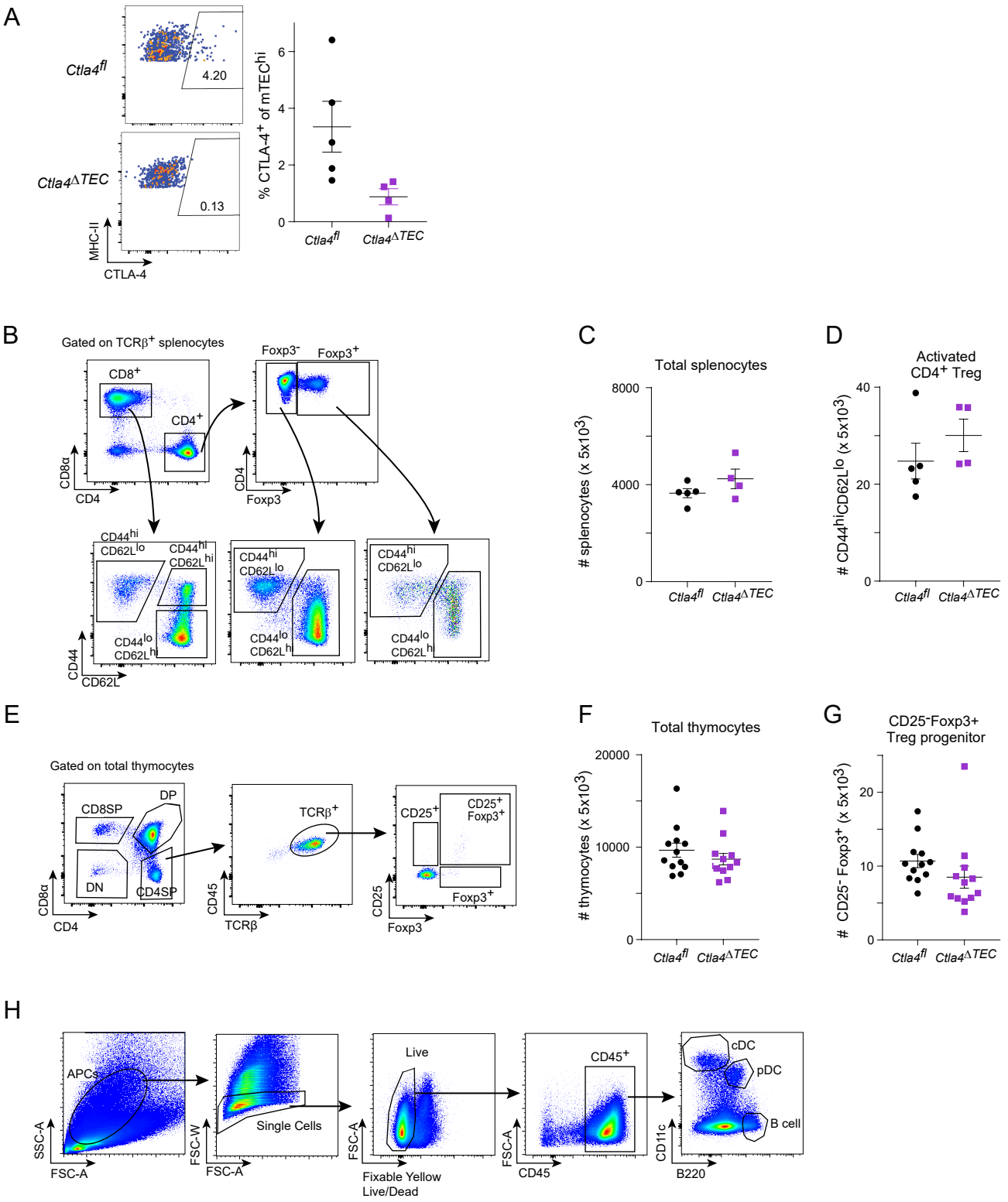

Supplementary Fig 3